Phase Plane and Bifurcation Analysis of Thin Wavy Films under Shear

A long-wave equation for film thickness as a function of position is derived for a general case incorporating viscous, surface tension, and interfacial shear effects. The derivation considers both the parabolic and the power-law velocity profiles. The analysis is aimed at revealing the wave velocity that induces infinitely long (homoclinic) periods as well as substrate thickness and wave peak amplitude. Phase plane analysis shows that at $Re \gg 1$, due to time-scale separation, the homoclinic velocity is near that at the Hopf bifurcation. That enables analytical derivation of the wave characteristics.

Comparison with experimental results in the range of Re-310-3,100 with countercurrent gas flow, shows encouraging agreement. At very high Re the wave velocity suggests the onset of turbulence, in agreement with theory. Phase plane analysis predicts also that the wave shape consists of a simple peak with a steep front, with short waves riding on the main wave at low Re.

M. Sheintuch, A. E. Dukler
Chemical Engineering Department
University of Houston
Houston, TX 77204

Introduction

The prediction of wave characteristics of falling liquid films has been the subject of numerous investigations (Dukler, 1977). Most studies have focused on free-falling films at low Reynolds number (Kapitza and Kapitza, 1949; Alekseenko et al., 1985) and have used linear stability analysis to determine the range of unstable wave velocities and the mode of the fastest growing wave. The film is assumed to be sinusoidal, oscillating about its mean value or even somewhat perturbed from a sinusoidal shape. This type of analysis predicts the wavelength and velocity at the conditions of wave inception. The long-wave approximation (Benney, 1966) considers the limit of very long and shallow waves that reach constant shape in the frame of a moving coordinate. Again, the wave evolves from the mean film thickness. Recent nonlinear analysis searched for wave velocities that induce infinitely long periodic solutions (homoclinic orbits). These studies were limited to falling films at low Reynolds numbers (Pumir et al., 1983) or used a questionable approximation for the flow condition (Needham and Merkin, 1984). Another approach, applied at high Re, is to approximate the wave shape by assuming a sequence of characteristic velocity profiles at different locations along the wave (Maron et al., 1985). Finally, numerical solutions of the evolution equation (Bach and Villadsen, 1984) did show the existence of constant-shape solitary waves. Even at Reynolds number of order 10 such computations are highly time consuming, and problems of numerical instability are encountered.

The purpose of this analysis is to present asymptotic solutions for wave velocities as well as certain dimensional characteristics of falling liquid films experiencing interfacial shear induced by gas flow. For this purpose methods of nonlinear analysis are used. Experiments have shown that at positions well below the plane of wave inception, two classes of waves exist on the surface (Dukler, 1977). Large waves can be observed riding on a thin substrate, with the ratio of peak wave height to substrate thickness ranging from 2 to 4. A second class of waves that are capillary in nature and of much smaller amplitude than the first is also present. These ride on the substrate and are sometimes seen on the trailing edge of the large waves. In the presence of gas flow parallel to the mean surface, interfacial shear is generated and the wave structure changes but the two wave class structure can still be seen. At sufficiently high countercurrent gas flow rates a condition of flooding can be reached where part of the liquid introduced on the vertical surface flows upward.

For complex problems such as this one, two rather divergent approaches are available. At low Reynolds numbers an analyti-

The current address of M. Sheintuch is: Chemical Engineering Department, The Technion, Haifa, Israel.

cal method is possible in the vicinity of certain singular points that can be shown to exist (Chang, 1986). For high Re a different approach is possible if it can be shown that the system is characterized by two or more widely different time scales. This paper takes the latter avenue, which has been largely unexplored. First we derive the integral momentum equation for the film under conditions of constant interfacial shear along the wave. Surface tension effects are incorporated and we assume alternatively a parabolic (laminar) or a power law (turbulent) profile. A complete analysis of the parabolic profile case is developed including interfacial shear while for turbulent flow the solution is explored only for free-falling films in the absence of gas flow.

The analysis strategy is then outlined and this is followed by the development of the solution to the flow equations for the two profiles, neglecting surface tension. For the parabolic profile it is shown that the shear makes no qualitative changes in the behavior of the system, having only a quantitative effect on the interfacial characteristics. As long as flooding is not induced the results are similar to those of the free-falling case. This same conclusion was reached by Zabaras and Dukler (1988) based on experimental observations. Turbulent flow may significantly reduce the wave velocity to a value approaching the mean liquid film velocity. Then the role of surface tension is explored. In the absence of surface tension an ordinary differential equation of the second order is generated and it is shown that the smooth film (Nusselt) solution cannot be a saddle point. When surface tension is added, a third-order ordinary differential equation is generated and every solution may be the saddle point and thus can be the source of the homoclinic orbit. The analysis of this complete form of the problem reveals that capillary waves can exist along the wave and substrate where the profile is flat, in addition to the large, long waves characterized by the homoclinic orbit; this too is in accord with experiment.

Finally, we compare the results with experiments of Zabaras and Dukler (1988).

The Film Equation

The Navier-Stokes equations are integrated in the direction y perpendicular to the wall, using both parabolic and power-law velocity profiles. The work may be extended to higher polynomial velocity profiles by numerical methods. We then apply a moving coordinate frame and arrive at one third-order equation for the film thickness.

Parabolic laminar profile

The film flowing downward under interfacial shear, τ_i, is described by

$$u_t + uu_x + vu_y = \frac{1}{\rho}(-P_x) + g + \nu(u_{xx} + u_{yy}) \tag{1}$$

$$u_x + v_y = 0 \tag{2}$$

subject to

$$u = v = 0 \quad \text{at} \quad y = 0 \tag{3}$$

$$u_y = \tau_i/\mu, \quad v = h_t + uh_x, \quad P = P_0 - \sigma h_{xx} \quad \text{at} \quad y = h \tag{4}$$

With integration in the y direction, Eq. 1 yields

$$Q_t + \frac{\partial}{\partial x}\int_0^h u^2\,dy = gh + \frac{\sigma h}{\rho}h_{xxx} + \nu\left[\int_0^h u_{xx}\,dy + \frac{\tau_i}{\mu} - u_y(0)\right] \tag{5}$$

with the local flow rate

$$Q = \int_0^h u\,dy \tag{6}$$

Assume a quadratic velocity profile that satisfies the conditions, $u = 0$ at $y = 0$; $\tau_i/\mu = du/dy$ at $y = h$; and $Q(h) = \int_0^h u\,dy$. This yields the following distribution function

$$u = \frac{Q}{h}\frac{3}{2}\eta(2 - \eta) + \frac{\tau_i}{\mu}\frac{h}{2}\eta\left(\frac{3}{2}\eta - 1\right) \tag{7}$$

with $\eta = y/h$. Clearly, this equation also describes the distribution in the undisturbed film (steady state) as well. With this distribution the following integrals can be evaluated.

$$\int_0^h u^2\,dy = \frac{6}{5}\frac{Q^2}{h} + \frac{Q\tau_i h}{20\mu} + \frac{h^3}{120}\left(\frac{\tau_i}{\mu}\right)^2 \tag{8}$$

From Eq. 6 the second x derivative of Q can be evaluated.

$$Q_{xx} = h_{xx}u(h) + h_x\frac{\partial}{\partial x}u(h) + h_x u_x(h) + \int_0^h u_{xx}\,dy \tag{9}$$

For the parabolic profile the last integral can then be evaluated.

$$\int_0^h u_{xx}\,dy = Q_{xx} - h_{xx}\left(\frac{3}{2}\frac{Q}{h} + \frac{1}{4}\frac{\tau_i}{\mu}h\right) - h_x^2\left(\frac{3Q_x}{hh_x} - \frac{3Q}{h^2} - \frac{\tau_i}{2\mu}\right) \tag{10}$$

Substituting these quantities into Eq. 5 gives the following equation for the case of constant shear independent of x.

$$Q_t + Q_x\left(\frac{12}{5}\frac{Q}{h} + \frac{1}{20}\frac{h\tau_i}{\mu}\right) + h_x\left(-\frac{6}{5}\frac{Q^2}{h^2} + \frac{Q\tau_i}{20\mu} + \frac{h^2}{40}\frac{\tau_i^2}{\mu^2}\right) = \left(g - \frac{1}{\rho}\frac{dP}{dx}\right)h + \nu\left(\int_0^h u_{xx}\,dy - \frac{3Q}{h^2} + \frac{3}{2}\frac{\tau_i}{\mu}\right) + \frac{\sigma h}{\rho}h_{xxx} \tag{11}$$

with $\int_0^h u_{xx}\,dy$ defined in Eq. 10. The integral of the continuity equation is

$$Q_x + h_t = 0. \tag{12}$$

Thus Eqs. 11 and 12 are two equations in h and Q as dynamic variables and x and t as independent variables. In a coordinate

frame moving with the wave velocity, c, set

$$\theta = t, \quad \xi = x - ct \tag{13}$$

and the mass conservation condition then becomes

$$h_\theta - ch_\xi + Q_\xi = 0 \tag{14}$$

The momentum balance, Eq. 11, can be modified by substituting $Q_\theta - cQ_\xi$ for Q_t, and $\partial^n/\partial\xi^n$ for ∂^n/dx^n. We make now two important assumptions:

1. The waves propagate without change in shape; thus in a moving coordinate system, $Q_\theta = h_\theta = 0$. Integration of Eq. 14 yields

$$Q - ch = K \tag{15}$$

where Q is the volumetric flow rate at any location ξ along the wave.

2. The integration constant, K should satisfy the steady state solution with $h = h_o$ and $Q = Q_F$, the liquid feed rate. Thus $K = Q_F - ch_o$. By integrating the velocity distribution over the steady state film thickness we find that

$$Q_F = \frac{gh_o^3}{3\nu}(1 + T) \tag{16}$$

with the dimensionless shear $T = 3\tau_i/2\rho g h_o$. Note that Eq. 16 may have more than one real solution for h_o given Q_F and τ_i, as discussed in detail by Maron and Dukler (1984). Substituting K calculated from the steady state solution, Eq. 15 becomes

$$Q = \frac{gh_o^3}{3\nu}(1 + T)[1 + n(H - 1)], \quad H = \frac{h}{h_o}, \quad n = \frac{ch_o}{Q_F} \tag{17}$$

where n is the wave velocity made dimensionless in respect to the average velocity. Substitution of Eq. 17 into the momentum balance, Eq. 11, yields an ordinary third-order differential equation describing the change of dimensionless film thickness, H, with dimensionless length $l = \xi/L$. The length scale, L, and dimensionless parameters are defined as

$$L = \frac{h_o Re}{1 + T} \quad Re = \frac{Q_F}{\nu} \quad W = \frac{\sigma}{\rho g^{1/3}(3\nu^2)^{2/3}} \tag{18}$$

The resulting equation is

$$\epsilon_1 H^3 H_{lll} + \epsilon_2[C_2(H)H_{ll} - C_3(H)H_l^2] + (1 + T)^2 C_1(H)H_l + C_0(H) = 0 \tag{19}$$

where

$$\epsilon_1 = \frac{27W(1 + T)^{11/3}}{Re^{11/3}} \quad \text{and} \quad \epsilon_2 = \frac{27(1 + T)^3}{Re^2}$$

In this development the dimensionless shear stress τ_i is assumed to be independent of the position along the wave l and the coefficients are:

$$C_0 = (H - 1)[H^2 - (T + 1)(n - H - 1)]$$

$$C_1 = -\frac{n^2}{5}\left(H - \sqrt{6}\frac{n-1}{n}\right)\left(H + \sqrt{6}\frac{n-1}{n}\right) - \frac{TH^2}{10(1 + T)}\left(2nH + 1 - n + \frac{TH^2}{1 + T}\right)$$

$$C_2 = H\left[\frac{3}{2}(n - 1) - \frac{nH}{2} - \frac{1}{2}\frac{H^2T}{1 + T}\right]$$

$$C_3 = 3(n - 1) - \frac{H^2T}{1 + T} \tag{20}$$

These equations apply for downflow of liquid with countercurrent gas flow ($g > 0$, $\tau_i < 0$, $-1 \le T \le 0$) or cocurrent flow ($g > 0$, $\tau_i > 0$, $T > 0$) as well as for upflow where x or l is positive in the flow direction ($g < 0$, $\tau_i > 0$, $T \le -1$); the inequality, $T \le -1$, follows from the requirement that Q_F be positive in Eq. 16.

A schematic representation of the relation between T and h_o as deduced from Eq. 16 appears in Figure 1 for constant Q_F. Downflow with countercurrent shear takes place for $-1 \le T \le 0$ (band B in the figure). However in the range $-3/4 < T < 0$ the velocities are directed uniformly downward at all locations in the film. For $T = -3/4$ the profile is symmetric, with zero velocity at the interface, and when $-1 < T < -3/4$, downward-directed velocities exist near the wall, with upward velocities near the interface. Band A in Figure 1 represents concurrent downward flow while band C displays the behavior for concurrent upward flow. In these bands, for the range $-1.5 < T < -1$, the velocity profile is again not monotonic. For more negative values of T uniformly upward flow exists in the film. *At* $T = -1.5$ the wall shear is zero and the upward motion of the liquid is driven by the interfacial shear only. The existence of these different patterns of velocity distribution was discussed by Maron and Dukler (1984) and their existence confirmed experimentally by Zabaras et al. (1986).

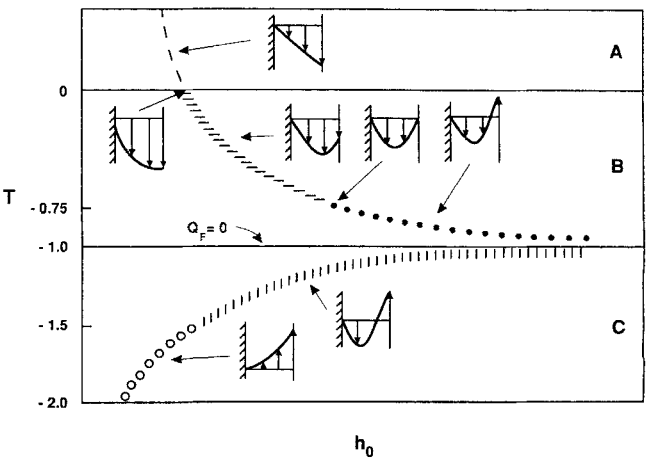

Figure 1. Solutions to steady state film thickness equation.

Turbulent profile in the absence of shear

For turbulent flow, the film velocity profile can be expressed in a power law form:

$$u = \frac{(1+\alpha)}{\alpha}\frac{Q}{h}\eta^{1/\alpha} \tag{21}$$

We find

$$\int_0^h u^2\,dy = \frac{(1+\alpha)^2}{\alpha(2+\alpha)}\frac{Q^2}{h} \qquad \int_0^h u\,dy = Q \tag{22}$$

The integral momentum equation then becomes:

$$h_t\left(-c^2 + \frac{(1+\alpha)^2}{\alpha(2+\alpha)}\frac{Q(2ch-Q)}{h^2}\right) = gh - \frac{\tau_w}{\rho} + \nu h_{\xi\xi}\left(c - \frac{(1+\alpha)}{\alpha}\frac{Q}{h}\right) + O(h_\xi^2) \tag{23}$$

$$Q - ch = Q_o - ch_o \tag{24}$$

For turbulent flow the wall shear stress τ_w cannot be approximated from the velocity profile and correlations are needed. As shown below, this has no influence on the dimensionless wave velocity but does change the mean film thickness and consequently the dimensional velocity. From the Blasius relation

$$\frac{\tau_w}{\rho} = \frac{1}{2}\bar{u}^2 \cdot \frac{\lambda}{8}; \quad \bar{u} = \frac{Q}{h} \tag{25}$$

where the friction factor at the wall, λ, is estimated from single-phase flow models.

$$\frac{\lambda}{8} = 0.056(Q/\nu)^{1/4} \tag{26}$$

When this relation is substituted into Eq. 24 for the flat film, we find

$$\frac{h_{o(\text{turb})}}{h_{o(\text{lam})}} = 0.21\,Re^{1/4} \tag{27}$$

In the application of Eq. 23 at high flow rates the value of α can be expected to vary along the wave. At the substrate the local flow rate is low, turbulence is suppressed, and the quadratic law will apply. In the thicker portions of the wave near the crest, turbulent behavior will result in increased values of α. Methods for accounting for this flow direction variation in α have not yet been fully implemented. As a first approximation we use a constant value of α for the dynamic analysis of the momentum equation.

Strategy of Dynamic Analysis

The dynamic equation for the film thickness, Eq. 19, contains four parameters, *Re*, *W*, *n*, and *T*, which are to be specified as input variables. Even though the slopes of the waves are known to be small it is not possible to simplify the equation by neglecting the H_{II} and H_{III} terms since these quantities are necessary to the stability and dynamic analysis that follows. Define the following dimensionless term

$$\beta = \frac{\epsilon_2}{\epsilon_1}(1+T)^2 = \frac{(1+T)^{4/3}Re^{5/3}}{W} \tag{28}$$

When β is large the inertial forces are large compared to the surface forces and the first term in Eq. 19 can be neglected.

The steady state solution of Eq. 19 is the space-independent ($H_I = H_{II} = H_{III} = 0$) solution of $C_0(H) = 0$. The qualitative nature of these solutions is shown in Figure 2 for different ranges of T. The unperturbed film ($H = 1$) is always a solution but there is always a range of velocities n for which it is not stable. The other two solutions, for any T, form a parabolic branch $n = H^2/(1+T) + (1+H)$ which intersects $H = 1$ at $n = (3+2T)/(1+T)$ and acquires a turning point at $H = -(1+T)/2$, $n = (3-T)/4$. The parabolas for upflow, Figure 2a, and downflow, Figure 2b, open in opposite directions. The range of values of n over which the $H = 1$ solution is unstable can be determined from linear stability analysis. Specifically, there will usually exist a (Hopf) bifurcation point, which is the value of n at which a transition to periodic behavior takes place and oscillations are observed in the frame of a moving coordinate; that is, waves propagate along the film in the physical system. The H–n diagram for $T = 0$ showing the nature of the various states as determined by linear stability analysis is shown in Figure 3. As the waves grow, their velocities vary in the direction of lower n (more unstable). The waves form a family of closed curves (limit cycles) in the phase plane (H_I vs. H) or phase space (H_{II}, H_I, H) and these closed curves increase in area as the waves grow in amplitude along the film in the coordinate direction. These waves have a peak such that $H > 1$ and a substrate thickness $H < 1$. As the wave grows the substrate becomes smaller. At the condition where the substrate thickness is equal to that of the saddle point the wave can grow no more and its velocity will not change. In the phase plane the largest possible wave will be formed when the limit cycle hits a saddle point forming a homoclinic curve. This curve provides the asymptotic amplitude of the wave and the corresponding velocity, n_s. Further change in n cannot take place since this results in the elimination of the oscillations. The wavelength of this form is infinite since the motion takes place in the vicinity of the saddle point, which is a steady state, and thus is infinitely long. The saddle point satisfies the steady state solution $C_0(H_3) = 0$.

The purpose of the nonlinear analysis is to determine the location, n_s, and form of the homoclinic curve (also termed saddle-loop bifurcation). That is possible analytically only in two cases:

1. In the small neighborhood of higher order singularities such as when Hopf and saddle-node bifurcations coalesce. Then

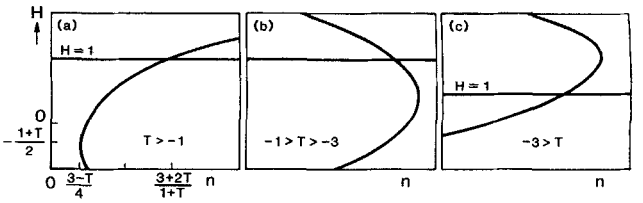

Figure 2. Variation of steady state film thickness with *n*.

a. Downflow; b, c. Upflow
Coordinates for limit points in (b) and (c) same as in (a)

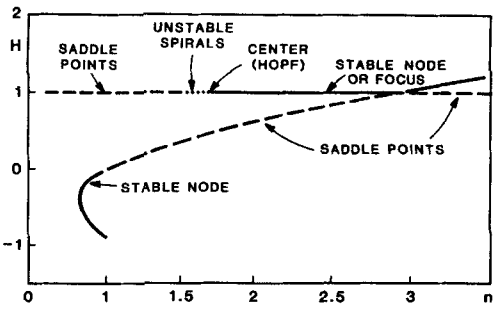

Figure 3. Changes in the nature of the steady states.
Determined from linear stability analysis for $T = 0$ and negligible surface forces

a. $n = n_H$; b. $n < n_H$
c. $n = n_s \rightarrow h_H$; d. $n > n_H$

the oscillations are infinitesimally small and can be described by perturbation of the linear solution.

2. When the system is characterized by different time scales.

We capitalize here on the latter property.

The dynamic analysis of Eq. 19 requires working in the three-dimensional phase space, H, H_I, H_{II}. However many of the essential dynamic features of the system can be discerned by analyzing the phase plane H, H_I. Equation 19 reduces to this problem for high Reynolds numbers when $\beta \rightarrow \infty$. Thus the procedure will be to first analyze the simplified system in the phase plane for both laminar and turbulent flow. Then the analysis will be generalized for cases where β is not large.

Laminar Film Flow for $\beta \rightarrow \infty$

In the case $W = 0$, Eq. 19 can be written in the form

$$H_I = w \tag{29}$$

$$\epsilon_2 C_2 w_I = -(1 + T)^2 C_1 w - C_0 + \epsilon_2 C_3 w^2 = f(H, w) \tag{30}$$

Linear stability analysis requires the determination of the eigenvalues of the Jacobian matrix $\partial(w, f/\epsilon_2 C_2)/\partial(H, w)$ at the steady state $H = 1$, $w = 0$. The matrix is then

$$J = \begin{pmatrix} 0 & 1 \\ \dfrac{f_h}{\epsilon_2 C_2} & \dfrac{f_w}{\epsilon_2 C_2} \end{pmatrix} \tag{31}$$

and the state may destabilize by one of two ways:

1. A Hopf bifurcation to periodic behavior occurs at

$$\text{tr } J = \frac{f_w}{\epsilon_2 C_2} = -\frac{(1 + T)^2 C_1(1)}{\epsilon_2 C_2(1)} = 0 \quad |J| > 0 \tag{32}$$

The state is unstable for $C_1(1)/C_2(1) < 0$, or from Eq. 20 with $T = 0$,

$$\frac{3}{2} < n < \frac{6}{5} + \frac{\sqrt{6}}{5} = n_H \tag{33}$$

2. Exchange of stability from $H = 1$ to the $H \neq 1$ solution occurs when

$$|J| = -\frac{f_H}{\epsilon_2 C_2} = \frac{C_{0H}(1)}{\epsilon_2 C_2} = 0; \quad C_{0H}(1) = \frac{dC_0}{dH}(1) \tag{34}$$

yielding $n = 3$ when $T = 0$, that is, at the intersection point of the two branches. These transitions are observed in Figure 3 where the unstable branches are marked by broken lines.

Oscillations (waves) exist for a certain range of n as shown in Eq. 33. We show now that when $\epsilon_2 = 27\ (1 + T)^3/Re^2 \rightarrow 0$ the wave velocity at the homoclinic orbit is very close to that at the Hopf ($n_s \rightarrow n_H$). Note that ϵ_2 does not affect the stability boundaries, Eq. 32, but it affects the behavior in the phase plane. From Eq. 30, with $T = 0$ and when the small $\epsilon_2 C_3 w^2$ term is ignored, the direction of the motion (slope in the $H - H_I$ plane) is

$$\frac{dw}{dH} = \frac{\dfrac{n^2}{5}(H - H_4)(H + H_4)w - (H - 1)(H - H_2)(H - H_3)}{\epsilon_2 w H \dfrac{n}{2}(-H + H_5)} = \frac{f(H, w)}{\epsilon_2 w C_2(H)} \tag{35}$$

where $H_{2,3}$ are the roots of $C_0(H) = 0$ with H_4 and H_5 defined from Eq. 20 after setting $T = 0$.

$$H_{2,3} = -0.5 \pm \sqrt{n - 0.75}$$

$$H_4 = \sqrt{6}\,\frac{n - 1}{n}$$

$$H_5 = \frac{3(n - 1)}{n} \tag{36}$$

Since ϵ_2 is small, $dw/dH \rightarrow \infty$ everywhere in the phase plane except when the numerator vanishes. At this condition of $f = 0$

$$w = \frac{(H - 1)(H - H_2)(H - H_3)}{\dfrac{n^2}{5}(H - H_4)(H + H_4)} \tag{37}$$

The shape of the w vs. H curves resulting from this expression are dependent on the velocity, n, since $H_{1\text{-}5}$ are functions of n. Figure 4a shows the solution of Eq. 37 at $n = n_H = 1.689$, Eq. 33. $H = 1$ is one branch of the solution for all w since $H_4 = 1$ at $n = n_H$. The second branch crosses this $H = 1$ branch and intersects the abscissa at H_3. We have already shown that for any point in the phase plane the trajectory must be vertical except near the $f = 0$ curves. Thus all trajectories starting at $H < 1$ flow toward the second branch except for those that originate in the immediate vicinity of the $H = 1$ line. Along the curves the trajectory must be horizontal. As the $f = 0$ lines are approached the trajectory must move along the $f = 0$ curve and increasingly close to it in direction. This direction is indicated in the usual way by heavy arrows on the solution branches. The sign of w_I is an indicator of the direction of the vertical trajectories. As seen in Eq. 30, this direction changes as $f(H, w)$ passes through zero. Similarly, the sign of H_I is an indicator of the direction of horizontal motion. Eq. 29 shows that this direction changes as w passes

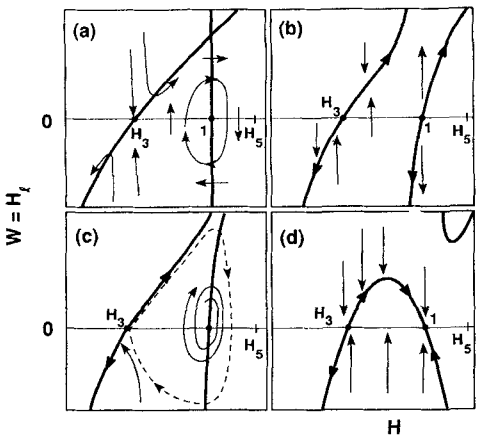

Figure 4. Phase-plane analysis of two-variable model.
Heavy lines, $f = 0$; thin lines, direction of motion

a. $n < n_H$; b. $n_H < n < n_s$
c. $n = n_s$ for $Re \to \infty$; d. $n = n_s$

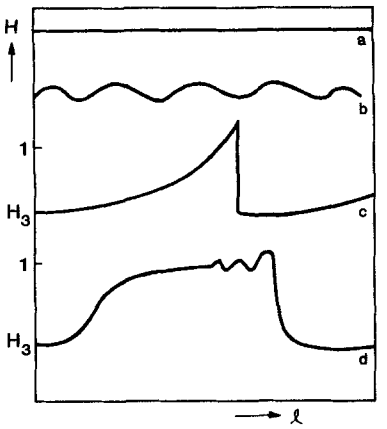

Figure 5. Qualitative sketch of wave profile.

through zero. Equation 35 shows that trajectories cannot cross the $H = H_5$ boundary since at this point $C_2(H) = 0$ and a discontinuous change in the direction of motion occurs. When this begins to happen the surface tension terms neglected here become important. Thus waves that initiate from the smooth film cannot achieve an amplitude greater than H_5.

Solutions of Eq. 37 for $n < n_H$ and $n > n_H$ appear in Figures 4b and 4d. In the latter case the steady state, $H = 1$, is stable and all trajectories in its vicinity are attracted there. For $n < n_H$ in Figure 4b, the steady state at $H = 1$ is unstable and all trajectories escape to infinity. Of particular interest is the case where $n \to n_H$, illustrated in Figure 4c. The Hopf theorem indicates that a limit cycle surrounds the unstable state, $H = 1$, near the condition for a Hopf bifurcation. Thus the situation appears as shown in Figure 4c for n somewhat less than n_H. Periodic oscillations wind out in a spiral from its origin at $H = 1$ and gradually grow in amplitude until they disappear in a homoclinic orbit at H_3.

Now it is possible to deduce that the value of n_s at which this takes place must be negligibly different from n_H when ϵ_2 is small. Under these conditions the trajectories are almost vertical, and the limit cycle must be narrow in the H direction and long in the w direction. If the two branches of the $f = 0$ curve are far apart, as they are when n is significantly lower than n_H, the trajectories can readily escape to infinity. As ϵ_2 increases, the trajectories continue to flow toward the left branch of the $f = 0$ curve but now they can travel a short distance, ϵ_2, away from these curves. The separation distance between the two $f = 0$ curves increases as $n_s - n_H$. Thus for the trajectory to move from $H = 1$ on one branch of $f = 0$ to H_3 on the other requires that $n_s - n_H$ be of the order of ϵ_2, a small number under the experimental conditions of interest here. Thus we conclude that $n_s = n_H$.

Pictures of the developing waves can be arrived at by analyzing the trajectory in the phase plane, as shown in Figure 5. The initially flat interface (a) displays small sinusoidal waves at the point of wave inception (b) with the wave velocity, $n = n_H = 1.689$, Eq. 33, at this condition. But the condition is unstable and the spiral unwinds around $H = 1$ to become a homoclinic orbit at $n = n_s$ in close proximity to n_H. In its homoclinic orbit the minimum or substrate wave amplitude is $H_3 = 0.47$ (Eq. 36 for $n = n_H$). H then increases rapidly at the front of the wave with high slope, w. As it approaches its peak amplitude the slope drops to zero. The peak cannot exceed $H_5 = 1.25$. Then the sign of the slope changes and along the back the wave tapers more slowly down to the substrate thickness, H_3.

The existence of countercurrent shear does not change this qualitative picture, modifying only the wave characteristics. Steady states are linearly unstable when $C_1(1)/C_2(1) < 0$ or

$$\left(\frac{3}{2} + \frac{s}{2}\right) < n < n_H = \frac{6}{5} + \frac{s}{20} + \frac{\sqrt{6}}{5}\sqrt{1 + \frac{22s}{24} + \frac{41s^2}{96}} \qquad (38)$$

where $s = T/(1 + T)$. The upper root of $C_1(1) = 0$ is n_H and this is the solution of

$$-\frac{n^2}{5}\left[1 - 6\left(\frac{n-1}{n}\right)^2\right] - \frac{s}{10}(1 + n + s) = 0 \qquad (39)$$

The other stability boundary, $J = 0$, occurs at $n = 3 - s$. A map of the linear stability appears in Figure 6 for downflow with countercurrent ($s < 0$) or cocurrent ($s > 0$) shear. The relative positions of the three boundaries are identical to those for the free-falling film problem. They intersect at $s = 1$, $n = 2$, which does not correspond to any physical situation ($T \to \pm\infty$). For upward flow ($T < -1$, $s > 1$) the relative positions of the three

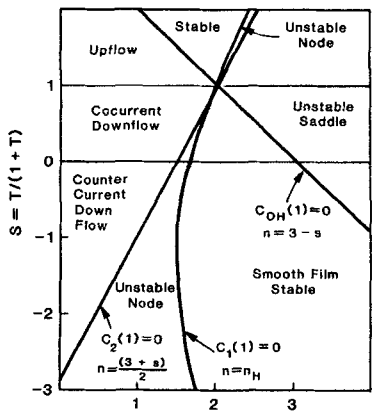

Figure 6. Stability map for smooth film in the presence of shear for two-variable case.

bifurcations are interchanged. The phase plane analysis for downflow with countercurrent shear is analogous to the $T = 0$ case. At $n = n_H$, $H = 1$ is a solution for any w and the $f = 0$ curve acquires the shape of Figure 4a. Changing n modifies the diagram in a similar fashion and we conclude again that a homoclinic orbit must exist close to n_H with the same general shape as in Figure 5. The substrate height, H_3, and the limiting wave amplitude, H_5, are given by

$$H_3 = \frac{-1 + \sqrt{1 + 4(n_H - 1)(1 - s)}}{2(1 - s)}$$

$$H_5 = \frac{-1 + \sqrt{n^2 + 12n - 1}}{2s} \tag{40}$$

This analysis shows the following behavior of the system for downflow with countercurrent shear

1. The wave characteristics depend on the shear parameter, T (or s)
2. The wave velocity, n, which approximates the velocity at the Hopf bifurcation, varies weakly with T (or s), taking on values of 1.69 at $T = 0$ ($s = 0$), 1.5 at $T = -\frac{1}{2}$ ($s = -1$), and 1.75 at $T = -\frac{3}{4}$ ($s = -3$)
3. The maximum wave amplitude increases markedly with countercurrent shear since H_5 increases as s becomes more negative

Extension of the analysis to upflow shows that the relative positions of the bifurcation points, Figures 2, 6, are arranged in a mirror image to the downflow case and the conclusions are thus similar for cocurrent flow. However the existence of multiple values of the equilibrium film thickness for any shear stress and flow rate as discussed above raises these additional issues:

1. Either one or both of these solutions may not be stable
2. The location of the turning point at $n = (3 - T)/4$ may be outside the domain where oscillations can exist

Turbulent Film Flow

The analysis of Eq. 19 for laminar film flow presented above showed that $C_1(H = 1) = 0$ is a necessary condition for instability (see also Figure 6). Note that C_1 is the coefficient of H_l, the slope of the wave in dimensionless form, and $H = 1$ is the condition for the smooth film, $h = h_o$, $Q = Q_F$. For turbulent flow the same condition can be shown to exist. Thus, the coefficient of the dimensional slope, h_ξ, in Eq. 23 must be zero, resulting in the following relation for the dimensionless wave velocity.

$$-n^2 + 2f(\alpha)n - f(\alpha) = 0 \quad f(\alpha) = \frac{(1 + \alpha)^2}{\alpha(2 + \alpha)} \tag{41}$$

or

$$n = f(\alpha) + \sqrt{f(f - 1)} \tag{42}$$

This result is independent of the particular form of the correlation used for the wall stress. At high flow rates, as the flow becomes more turbulent α increases and n approaches 1.0. Thus for a velocity distribution that follows a 1/7th power law, $n = 1.14$. It should be noted that such low values of the wave velocity cannot be predicted from any laminar distribution but have been observed experimentally for high flow rates, Eq. 12.

Laminar Films with Surface Forces: General Case

When surface tension effects are retained in the model a general form of Eq. 19 can be written as follows where $w = H_l$ and $\phi = w_l$:

$$\phi_l = \frac{f(H, w) - \epsilon_2 C_2 \phi}{\epsilon_1 H^3} = \frac{g(H, w, \phi)}{\epsilon_1 H^3} \tag{43}$$

where $w = H_l$ and $\phi = w_l$ and $f(H, w)$ is defined in Eq. 30. The Jacobian matrix at $H = 1$, $w = \phi = 0$ is:

$$J = \begin{pmatrix} 0 & 1 & 0 \\ 0 & 0 & 1 \\ -\dfrac{C_{0H}(1)}{\epsilon_1} & -\dfrac{C_{1H}(1)}{\epsilon_1} & -\dfrac{\epsilon_2}{\epsilon_1} C_2(1) \end{pmatrix} \tag{44}$$

The characteristic equation, $|J - \lambda \bar{\bar{I}}| = 0$, is

$$\lambda^3 + \frac{\epsilon^2}{\epsilon_1} C_2(1)\lambda^2 + \frac{(1 + T)^2 C_1(1)}{\epsilon_1}\lambda + \frac{C_{0H}(1)}{\epsilon_1} = 0 \tag{45}$$

and its roots are the eigenvalues that determine the stability. Applying Routh-Hurwitz stability criteria reveals that $H = 1$ is stable ($\lambda_1, \lambda_2, \lambda_3 < 0$) if the following three conditions are satisfied

(a) $C_{0H}(1) > 0$

(b) $C_2(1) > 0$

(c) $$\frac{C_{0H}(1)}{\epsilon_1} - \frac{(1 + T)^2 C_1(1) C_2(1) \epsilon_2}{\epsilon_1^2} > 0 \tag{46}$$

Condition (a) is the exchange of stability, described earlier, and it implies $n < 3 - s$. Condition (b) is also unchanged, requiring $n > (3 + s)/2$. Hopf bifurcation occurs when condition (c) is violated and the bifurcation points depends now on the ratio of the viscous to surface tension terms. It reduces either to the previous Hopf condition ($C_1 = 0$) when $\epsilon_2/\epsilon_1 \to \infty$ or to condition (a) when $\epsilon_2/\epsilon_1 \to 0$. Substituting the relations for the $C_i(H)$, Eq. 20, we find that Hopf bifurcation ($n = n_H$) occurs at

$$\beta = \frac{(1 + T)^{4/3} Re^{5/3}}{W}$$

$$= \frac{(3 - s - n)10}{\left(n - \frac{3}{2} - \frac{s}{2}\right)[-2n^2 + 12(n - 1)^2 - s(1 + n + s)]} \tag{47}$$

The nature of the steady state is shown in the (β, n) plane of Figure 7 by denoting the sign of the three eigenvalues. Limit cycles may exist in the range $(3 + s)/2 < n < n_H$ and the order of the various points is unaffected by changing T for downward flow.

Analysis of the trajectories in the three-dimensional space (H, w, ϕ) is more intricate than the two-dimensional version. The structure of the analysis follows. We investigate the shape of the $g = 0$ surface, Eq. 43, in the phase space to show that it attracts the motion and ask: is the motion along it stable? It

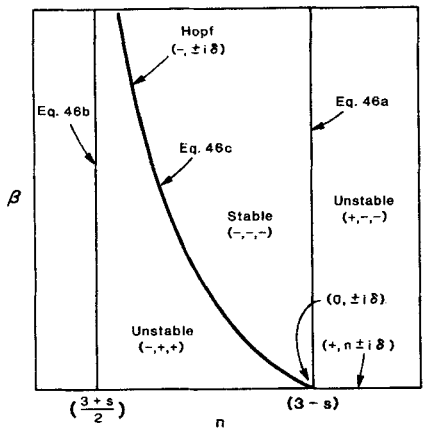

Figure 7. Stability map for general case.

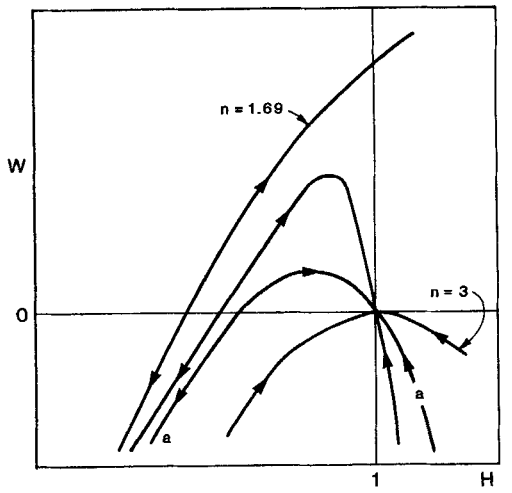

Figure 8. Family of $f = 0$ curves in w–H plane.

turns out that it is unstable in certain sections. We find the stable and unstable manifold and construct the trajectory in space. The steady state $H = 1$ may be the origin of the homoclinic orbit. It has a stable one-dimensional (i.e., a line) manifold and an unstable two-dimensional (surface) manifold along which the motion spirals. These spirals yield the capillary wave and are evident only with relatively small Re (ϵ_1/ϵ_2 large). After it spirals out, the trajectory travels in the vicinity of H_3 so that the dimensionless value of the film thickness is still a good approximation for the substrate thickness.

The slopes of the trajectories can be found readily from Eq. 43 to be:

$$\frac{d\phi}{dH} = \frac{g}{\epsilon_1 H^3 w} \quad \frac{d\phi}{dw} = \frac{g}{\epsilon_1 H^3 \phi} \tag{48}$$

Note that $\epsilon_1 \to 0$ except for the lowest Reynolds numbers. Therefore the slopes of the trajectories in both the $\phi - H$ and $\phi - w$ planes are steep everywhere in the phase space except where $g \to 0$ or when the first and second derivatives of the wave profile, w and ϕ, are large. Data show that these derivatives are everywhere very small indeed. Therefore we now explore the region around $g = 0$.

From the definition for g in Eq. 43, when $g = 0$

$$\phi = \frac{f(H, w)}{\epsilon_2 C_2(H)} \tag{49}$$

For $\epsilon_2 = 0$ this implies that $f = 0$, a situation that was explored earlier. This can be pictured as a cylindrical surface in the phase space perpendicular to the $w - H$ plane. Figure 8 shows $f = 0$ curves for a sequence of values of n as determined from Eq. 37. The case for $n = 1.69$ appeared earlier in Figure 4a where it was shown that the crossing of the abscissa marks the location of H_3, the substrate height. Note that when $n = 3$ the value of H_3 becomes identical with the smooth film thickness, a condition in agreement with the experiment.

Figure 9 pictures the cylindrical surface, $g = 0$, in the phase space ϕ, w, H for $\epsilon_2 = 0$. When ϵ is small but not zero the surface is tilted somewhat. All trajectories starting from any point in the phase space not on $g = 0$ rapidly approach this plane since $\partial\phi/\partial H$ and $\partial\phi/\partial w$ are large. This is evident from Eq. 48 for the condition $\epsilon \to 0$. Once the trajectory reaches the $g = 0$ surface it can be described by the relations

$$H_l = w \quad w_l = \phi = f/\epsilon_2 C_2(H) \tag{50}$$

This is identically the two-dimensional model developed earlier, but the question of stability at any position on the surface must still be explored.

Suppose $H_o(l)$, $w_o(l)$, $\phi_o(l)$ is the solution to Eq. 43 along $g = 0$ with perturbations from this motion $\tilde{H} = H(l) - H_o(l)$, $\tilde{w} = w(l) - w_o(l)$ and $\tilde{\phi} = \phi(l) - \phi_o(l)$ described by

$$\tilde{H}_l = \tilde{w} \quad \tilde{w}_l = \phi \quad \epsilon_1 H^3 \tilde{\phi}_l = g_H \tilde{H} + g_w \tilde{w} + g_\phi \tilde{\phi} \tag{51}$$

Assume that perturbations in H are small and grow slowly so that $g_H = \partial g/\partial H$ can be averaged, and $\langle g_H \rangle$, $\langle g_w \rangle$, and $\langle g_\phi \rangle$ replace the original time-dependent g_H, g_w, g_ϕ. The motion is stable if the trivial solution of Eq. 51, $\tilde{H} = \tilde{\phi} = \tilde{w} = 0$ is stable, that is, if the eigenvalues are all negative. We do a stability analysis similar to that leading to Eq. 46 to find the stability condition

$$-\frac{\langle g_H \rangle}{\epsilon_1 H^3} - \frac{\langle g_\phi \rangle \langle g_w \rangle}{H^6 \epsilon_1^2} < 0 \tag{52}$$

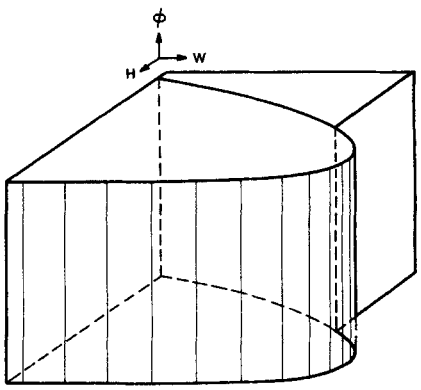

Figure 9. $g = 0$ surface in phase plane.

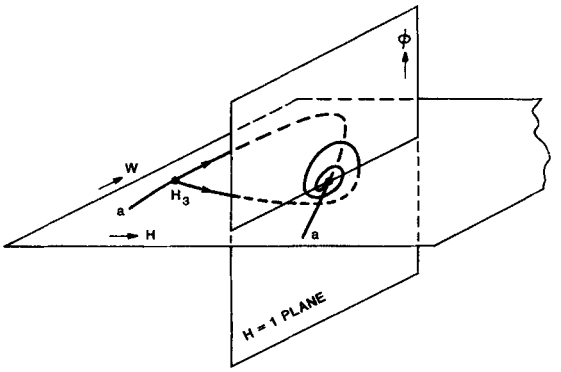

Figure 10. Trajectory of limit cycle.

or

$$\frac{\epsilon_2}{\epsilon_1}\frac{C_2}{H^3} > \frac{\partial}{\partial H}\left(\frac{C_0}{C_1}\right) = -\left(\frac{dw}{dH}\right)_{f=0} \tag{53}$$

An analysis of this equation shows that the transition occurs at $H = 1$. The section $H < 1$ is stable and is the stable manifold near $H = 1$. The motion around $H > 1$ is unstable and the trajectory oscillates around the line $f = 0$.

We now describe the motion in the vicinity of $H = 1$ with $n \sim n_H$. The stable manifold is the portion of the curve $f = 0$, denoted *aa* in Figure 10, that connects the H_3 and $H = 1$ solutions, denoted *ABC*. Its trajectory flows toward the steady state. At $n = n_H$ (Hopf point) there is a pair of imaginary eigenvalues and one negative eigenvalue:

$$\lambda_1 = -\frac{\epsilon_2}{\epsilon_1}C_2(1), \quad \lambda_{2,3} = \pm i\left(\frac{(1+T)^2 C_1(1)}{\epsilon_1}\right) \equiv \pm i\delta \tag{54}$$

The oscillations develop or decay with a period of $\sim(\epsilon_1/C_1(1))^{1/2}$. Since $C_1(1) \sim O(\epsilon_1/\epsilon_2)$ short periods of $O(\sqrt{\epsilon_1})$ are expected when the surface tension is important, while when surface tension effects are negligible the period is of $O(\sqrt{\epsilon_2})$. The eigenvectors that correspond to these imaginary eigenvalues were calculated to be $\phi = \delta^2(H-1)$ and $\phi = \pm i\delta w$; they define the unstable manifold. We note however that $\delta^2 \to \infty$ as $\epsilon_1 \to 0$ or $\epsilon_2 \to 0$. Thus $\delta^2(H-1)$ is finite only for $H = 1$. The plane $H = 1$ is thus a good approximation for the unstable manifold. For n somewhat smaller than n_H, λ_1 does not change significantly, while $\lambda_{2,3} = \Psi \pm i\delta$. The frequency is of order $\epsilon_1^{-1/2}$ or $\epsilon_2^{-1/2}$ as before and Ψ is the amplitude growth rate, which is small for high surface tension and large at the other extreme. For extremely small values of $(n_H - n)$ a limit cycle exists and it lies close to the $H = 1$ plane. Further increase in $(n_H - n)$ will break the cycle and the trajectory is detached from the plane and moves fast toward the stable manifold ($f = 0$). The resulting motion in Figure 10 shows a closed curve composed of a spiraling motion on $H \sim 1$ followed by a loop that travels around H_3. In the time domain we find small capillary waves whose number

Table 1. Wave Characteristics of Free-Falling Film ($T = 0$)

					n		Substrate	
Re	β	h_0 mm	Q_F/h_0 cm/s	c cm/s	Meas.	Theory	Meas.	Theory
78	1.18	0.28	28.2	68	2.58	2.46	0.8	0.75
192	0.26	0.39	50.3	105	2.14	2.10	0.72	0.72
387	0.08	0.50	76.8	120	1.49	1.77	0.66	0.62
778	0.025	0.63	127.0	140	1.10	1.70	—	0.47

Table 2. Measured Conditions Along Flooding Curve

Re	τ_i N/m²	$-T$	$-s$	c cm/s	n	h_s cm
15	3.29	0.9778	44.1	35.3	11.4	0.017
25	3.28	0.9662	28.5	43.8	9.05	0.0215
43	3.32	0.9237	12.1	50.0	6.29	0.024
63	3.49	0.9041	9.4	58.2	5.31	0.026
78	3.25	0.8906	8.1	61.6	3.60	0.029
109	3.59	0.8722	6.8	56.0	3.20	0.030
189	3.80	0.8309	4.9	86.9	3.14	0.037
298	3.98	0.7702	3.35	96.36	2.56	0.042

varies like ϵ_1/ϵ_2, Figure 5. The trajectory disappears when it hits H_3, which is still a good approximation for substrate thickness.

This analysis of the general third-order equation showed again that n_H and H_3 are good approximations for wave velocity and substrate thickness, respectively, but that the wave shape differs from that of the second-order model.

Comparison with Experiments

Experimental data on wave structure on falling liquid films with counterflow of gas were recently presented by Zabaras and Dukler (1988). These data are used here to evaluate this model.

Free-falling film

Equation 47 with $s = 0$ can be used to determine n_H, the dimensionless wave velocity at the Hopf bifurcation, and this can be compared with the experimental values to test the conclusion of the phase space study that this must be close to the velocity of the homoclinic orbit and thus to experimental data. Similarly, Eq. 40 provides a value of H_3, the minimum possible film thickness computed from the theory. This can be used to compute the substrate thickness, which can be compared with the data. These comparisons with the data of Zabaras and Dukler (1988) appear in Table 1; surprisingly good agreement is displayed considering the difficulty in experimentally determining the substrate thickness. It should be noted that the Reynolds

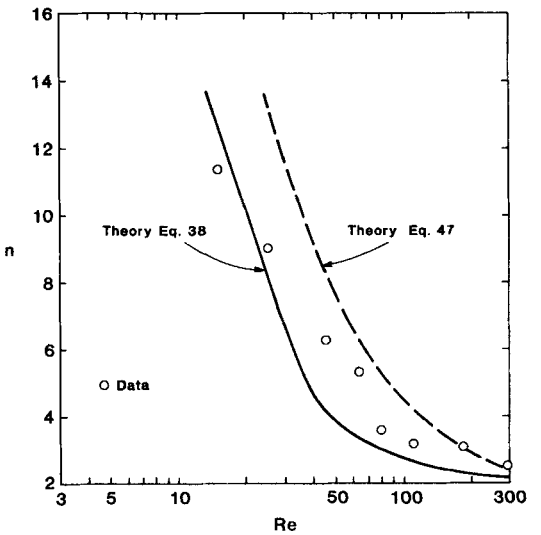

Figure 11. Theory-experiment comparison for wave velocity along flooding curve.

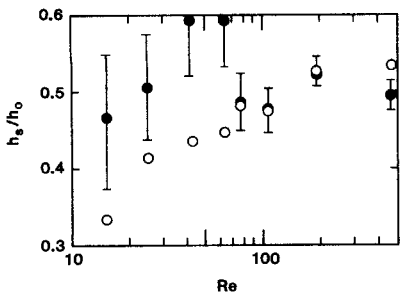

Figure 12. Theory-experiment comparison for substrate thickness along flooding curve.
○ Theory; ● Experiment

numbers in this work are defined as one-fourth those in the Zabaras and Dukler paper.

At Reynolds number above about 300 turbulent flow is thought to set in, the shape of the velocity profile changes, and the wave velocity would be expected to decrease, as discussed earlier.

Film with countershear

A severe test of the model is a comparison with data taken under the condition of interfacial shear due to counterflow of gas. Table 2 lists some original source data taken from the thesis of Zabaras (1985) during experiments along the flooding curve. Note that in accordance with theory the value of the dimensionless interfacial shear, T, is never less than -1. However at low liquid rates it approaches it closely. Figure 11 compares the experimental values of n with n_H calculated from the simple form of the equation in the limit $\beta \rightarrow 0$, Eq. 38, and from the general analysis, Eq. 47. The comparison is most encouraging, especially considering the fact that when $T \rightarrow -1$, the computed value of $s = T/(1 + T)$ used in both of these equations is extremely sensitive to small errors in T.

Not quite so satisfactory a comparison is shown in Figure 12. Here the dimensionless thickness calculated from Eq. 40 is compared with the dimensionless substrate thickness. The experimental values of s and n were used as input to these calculations. The error bars on the result due to the sensitivity of s to errors in T at the low flow rate is indicated. However it is still clear that the theory is not quite accurate enough in this region. We suspect this deviation is due to the assumption that the interfacial shear stress is independent of position along the interface and thus is the same over the substrate as it is over the wave itself. Experiments suggest that this is not the case and we are now exploring revised models which incorporate shear stress variation along the wave.

Acknowledgment

Financial support by the United States Office of Naval Research is gratefully acknowledged.

Notation

C_i = functions, Eq. 20
c = dimensional wave velocity
D = pipe diameter
f_0, f_1 = parameter in τ_i correlations, Eq. 58
f, g = functions, Eqs. 30, 43
h, H = dimensional, dimensionless film thickness
h_o, h_N = smooth film solution with, without shear
J = Jacobian matrix
l = dimensionless coordinate ξ/L
L = length scale $h_o Re/(1 + T)$
N = wave number
n = dimensionless wave velocity ch_o/Q_F
n_H, n_s = n of the Hopf and homoclinic saddle-loop bifurcations
P = pressure
Q, Q_F = local and feed liquid volumetric flow rate
Re = Reynolds number, Q/ν
s = modified shear parameter $T/(1 + T)$
T = dimensionless interfacial shear, $3\tau_i/2\rho g h_o$
t = time
U_G = linear gas velocity
u, φ = liquid velocity parallel, perpendicular to wall
w = dH/dl
W = surface tension parameter, Eq. 18
W_G, W_F = gas, liquid mass flow rate
x, y = coordinates in direction parallel, perpendicular to wall

Greek letters

α = exponent in power law profile, Eq. 21
β = ratio of time scales, Eq. 47
ν = kinematic viscosity
ρ = density
τ_i = shear at interface
σ = surface tension
η = dimensionless coordinate, y/h
μ = viscosity
θ, ξ = time, distance in a moving frame
ϵ_1, ϵ_2 = dimensionless time scales in terms H_{III}, H_{II}, defined following Eq. 43
ϕ = d^2H/dl^2
λ = eigenvalues of Jacobian matrix

Subscripts

x, y, H, etc. = derivative with respect to denoted quantities

Literature Cited

Alekseenko, S. V., V. Ye, Nakoryakov and B. G. Pokusaer, "Wave Formation on a Vertical Falling Liquid Film," *AIChE J.*, **31**, 1446 (Sept., 1985).

Bach, P., and J. Villadsen, "Simulation of the Vertical Flow of a Thin, Wavy Film Using a Finite-Elements Method," *Int. J. Heat Mass Transfer*, **27**, 815 (1984).

Benney, D. J., "Long Waves on Liquid Films," *J. Math Phys.*, **45**, 150 (1966).

Bharanthan, D., "Air-Water Countercurrent Annular Flow in Vertical Tubes," *Elec. Power Res. Inst. Rept.* EPR1 NP-786 (1978).

Chang, H. C., "Nonlinear Waves on Liquid Film Surfaces. I: Flooding in a Vertical Tube," *Chem. Eng. Sci.*, **41**, 2463 (1986).

Chu, K., and A. E. Dukler, "Statistical Characteristics of Thin Wavy Films. III," *AIChE J.*, **21**, 583 (Aug., 1975).

Dukler, A. E., "The Wavy Gas Liquid Interface," *Chem. Eng. Educ.*, 108 (1976).

———, "The Role of Waves in Two-Phase Flow" ASEE Award Lecture, *Chem. Eng. Educ.*, 108 (1977).

Kapitza, P. L., and S. P. Kapitza, "Wave Flow of Thin Layers of a Viscous Fluid," *Zh. Exper. i Teor Fiz.*, **19**, 105 (1949); also in coll. papers of P. L. Kapitza, Macmillan, New York (1964).

Maron, D. M., and A. E. Dukler, "Flowing and Upward Film Flow in Tubes," *Int. J. Mult. Flow*, **10**, 599 (1984).

Maron, D., N. Brauner, and A. E. Dukler, "Interfacial Structure of Thin Falling Films: Piecewise Modeling of the Waves," *Physicochem. Hydrodyn.*, **6**, 87 (1985).

Needham, O. J., and J. H. Merkin, "On Roll Waves Down an Open Inclined Channel," *Proc. Roy. Soc. London*, **A394**, 259 (1984).

Pumir, A., P. Manneville, and Y. Pomeau, "On Solitary Waves Running Down an Inclined Plane," *J. Fluid Mech.*, **135**, 27 (1983).

Zabaras, G. J., "Studies of Vertical Cocurrent and Countercurrent Annular Gas-Liquid Flows," Ph.D. Thesis, Univ. Houston (1985).

Zabaras, G. J., and A. E. Dukler, "Countercurrent Gas-Liquid Annular Flow Including the Flooding State," *AIChE J.*, **34**, 389 (Mar., 1988).

Zabaras, G., A. E. Dukler, and D. M. Maron, "Vertical Upward Cocurrent Gas-Liquid Flow," *AIChE J.*, **32**, 829 (May, 1986).

Manuscript received May 16, 1988 and revision received Sept. 26, 1988.